Archives of Hydro-Engineering and Environmental Mechanics
Vol. 45 (1998), No. 1–4, pp. 45–76

Bedload Transport Due to Waves Versus Laboratory Experiments

Leszek M. Kaczmarek*, Brian A. O'Connor, Ryszard B. Zeidler***

*Institute of Hydro-Engineering of Polish Academy of the Sciences, ul. Kościerska 7, 80–952 Gdańsk, Poland

**University of Liverpool, Dept. of Civil Engineering, Brownlow Street, P.O. Box 147, Liverpool L69 3 Bx, Great Britain

(Received September 17, 1998; revised November 28, 1998)

Abstract

The transport of sediment as bedload under wave action is studied both theoretically and experimentally. A theoretical approach based on grain-grain interaction ideas is proposed in analogy to the flow of dry, cohesionless materials. Nearbed sediment dynamics is modelled in two regions i.e. a collision-dominated granular-fluid region and a bed-bounded turbulent fluid shear region with continuous profiles of stress and velocity connecting both regions. An iteration procedure is employed to match the velocity and shear stress profiles in both regions using a theoretical bed level for the outer wave-induced flow of δ_{sx}, which is taken as an arbitrary fraction of the thickness of the moving, collision-dominated bed layer, δ_n. Previous comparisons with experimental data had suggested a value of $\delta_{sx}/\delta_n = 0.5$. The model has been operated for a range of sediments and for both low and high wave conditions. Comparison of model results with a range of experimental data suggests that the model provides realistic answers for both bed roughness and bedload transport thicknesses and rates for flat bed conditions provided variable values of $\delta_{sx}/\delta_n \leq 0.50$ are used. For sheet-flow conditions realistic values for bed roughness, bedload concentration and transport rate are obtained for $\delta_{sx}/\delta_n = 0.50$, although further model modifications are required to include the effects of suspended load. Finally, the model was found to produce realistic values of bed roughness and sediment transport rates for rippled bed conditions, provided $\delta_{sx}/\delta_n = 0.50$, which provides a measure of compensation for form drag, which is not explicitly included in the model.

Notation

a_{1m} – amplitude of water particle at the top of the wave boundary layer,

c – volumetric solid concentration,

c_0 – solid concentration corresponding to bed fluidisation,

c_m – solid concentration corresponding to a stationary, closely packed bed,

c_{ms} – solid concentration at which the bed would shear freely,

d – grain diameter,

d_{50} – median grain size,

$f_{2.5}$ – grain roughness friction factor,

f_w – wave friction factor,

g – acceleration due to gravity,

h – water depth,

k_a – apparent roughness height (laboratory data),

k_e – effective roughness height (used in computer model),

L_B – vertical scale of bedload distribution,

$L_{B\max}$ – L_B calculated for maximum shear stress,

L_t – time-averaged load defined as the time-averaged concentrations integrated over depth,

Q_B – bedload transport rate,

s – relative sediment density, ρ_s/ρ,

S_r – fluid-sediment interaction parameter defined as $S_r = \theta(d)/\theta_c$,

T – wave period,

u_0 – fictitious slip velocity at the nominal bed level,

u_b – apparent slip velocity at the nominal bed level,

u_f – total shear velocity,

$u_{f\max}$ – maximum total shear velocity during the wave period,

u_s – slip velocity at the theoretical bed level,

$u_{s,\max}$ – maximum slip velocity at the theoretical bed level,

U – free stream velocity,

U_{1m} – maximum free stream velocity,

z_1 – time-dependent variable defined as $z_1(t) = U\kappa/u_f$,

α_0 – constant defined as $\alpha^0 = \rho_s g d$,

δ – wave boundary layer thickness,

δ_n – level at which c equals c_{ms},

δ_s – ordinate indicating zero velocity level (bedload thickness),

$\delta_{s,\max}$ – bedload thickness for maximum shear stress,

δ_{sx} – limit of the downward extension of the turbulent velocity distribution from the theoretical bed level,

θ – dimensionless total shear stress (Shields parameter),

$\theta_{2.5}$ – grain Shields parameter with grain roughness friction factor $f_{2.5}$,
θ_c – critical Shields parameter (≈ 0.05),
$\theta_{\max}$ – Shields parameter for maximum shear stress during the wave period,
$\theta_{\max(d)}$ – Shields parameter for maximum shear stress based on bed roughness $k_e = d$,
$\theta_{\max(2.5d)}$ – Shields parameter for maximum shear stress based on bed roughness $k_e = 2.5d$,
κ – von Karman constant,
μ_0, μ_1, μ_2 – functions of the solid concentration,
ρ – water density,
ρ_s – grain density,
σ' – average normal stress,
σ_{ij} – stress tensor in granular shear region,
σ_{ij}^0 – plastic stress tensor,
σ_{ij}^* – viscous stress tensor,
τ – bed shear stress (total),
τ' – effective (skin) bed shear stress,
τ'' – bed shear stress arising from form drag,
τ''' – bed shear stress due to grain interactions,
φ – quasi-static angle of internal friction,
ϕ_B – dimensionless bedload transport rate,
$\phi_{B\max}$ – dimensionless bedload transport rate calculated for maximum bed shear stress,
$\phi_{T/2}$ – dimensionless bedload transport rate averaged over $T/2$,
ψ – angle between the major principal stress and x'-axis,
ψ_1 – constant determined as $\psi_1 = [(a_{1m}\omega)^2]/[(s-1)gd]$,
ω – angular frequency.

1. Introduction

Sediment transport due to surface waves is a complex physical phenomenon, in which are pronounced near-bed interactions between the wave-induced water motion and the sea-bed. The complexity becomes accentuated if the bed is porous and moveable. The problem is also extremely complicated because of the non-linearity of the near-bed interactions.

Proper understanding of wave-induced bedload dynamics requires a knowledge of the behaviour of sand grains in the collision-dominated, high-concentration

near-bed region, particularly at high shear stresses and sediment transport intensities when the near-bed sediment transport is known to take place in a layer with a thickness that is large compared to the grain size. The flow in the bed layer may not, therefore be described properly by conventional engineering models in which bedload transport is assumed to occur in a layer with a thickness of the order of one or two grains in diameter.

The present level of understanding of granular flow, which is influenced by grain inertia effects, owes much to the now-classical papers of Bagnold (1954, 1956). His work was motivated by an interest in the mechanics of sediment transport, including bedload transport in rivers. He derived simple equations to explain the rheological behaviour for two regimes, termed macroviscous and grain-inertia. In a macroviscous regime, viscosity of the interstitial fluid is dominant and the shear and normal stresses are linear functions of the velocity gradient, while in a grain-inertia regime the interstitial fluid plays a minor role and the major effects are due to particle-particle interactions.

In flows of dry, particulate solids, the fluid phase can be neglected for almost all values of the shear rate. At large shear rates, grain-inertia type of flow is to be expected. For very small shear rates and high concentrations of solids, a quasi-static deformation of the cohesionless soil is to be expected and not the behaviour associated with Bagnold's macroviscous flow. A "transitional region" joining the quasi-static type of flow to the grain-inertia flow clearly must exist.

The major purpose of the present study is to shed light on near-bed phenomena and interactions, with *emphasis on sediment transport as bedload.* Use will be made of earlier research by the first author, who postulated a mathematical model of bedload sediment transport in the sheet flow regime ignoring suspended load contributions (cf. Kaczmarek 1991, Kaczmarek & O'Connor 1993a, b).

In the sheet flow model, the near-bed dynamics was modelled for flow regions above and beneath the original static bed line. Figure 1 provides an explanatory drawing, with stresses on the left and velocities and concentrations on the right. The collision-dominated granular-fluid region I stretches below the nominal static bed while the wall-bounded turbulent fluid region II extends above it. Since both water and sand grains are assumed to move in both regions, there must be a certain transition zone between regions I and II, in which the velocity and stress profiles of regions I and II merge and preserve continuity of shape. The lower boundary of region II was positioned at $y_0 = k_e/30$, the height where the logarithmic velocity profile extrapolated from region II approaches zero, and the flow at the top of the transition zone was assumed to be unaffected by the transition phenomena. For analysis purposes, a theoretical bed level was chosen at δ_{sx} above y_0, the quantity δ_{sx} being an arbitrary fraction of δ_n, i.e. the thickness of the layer below the theoretical bed layer down to the lowermost immobile edge of region I. It was assumed that grain interaction effects were predominant in the lower layer (region I) while standard fluid dynamics determined the flow in region II.

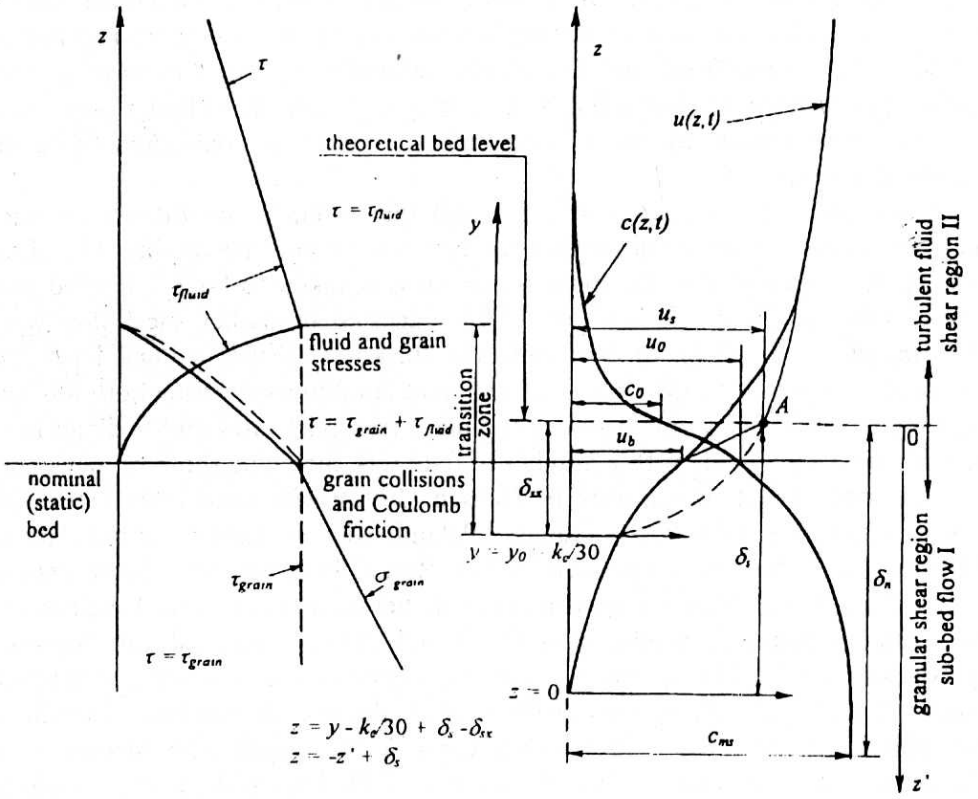

Fig. 1. Definition sketch

Making use of Bagnold's definition, which treats the bedload as a part of the total load supported by intergranular forces, it was assumed that the bedload layer was confined to the sub-bed flow region shown in Figure 1. Sayed & Savage (1983) stress tensor concept was also used for the description of the effective stresses inside the sub-bed flow region and following Einstein (1950), it was further assumed that bed slope effects were small in modifying sediment transport rate in the bedload layer.

The concept shown in Figure 1 is for moveable flat beds. Flat beds of loose sand under waves may offer considerably more resistance to the flow than sand paper with the same grain size. This is a consequence of the momentum transfer by moving sand from the flow to the bed. For rippled beds, it is, however, a more difficult concept to deal with. The total bed shear stress τ may be assumed to consist of three contributions namely, a form drag, τ'', a skin friction drag, τ', and a drag due to moving sand, τ'''. The significance of each of these for sediment transport is quite different. The form drag is generated by the difference

in pressures between the upstream and the downstream sides of bed forms, and it is assumed that there is no direct effect on the stability of individual surface sediment particles. The main disturbing influence on the surface grains is generally considered to come from the skin friction component τ' and to moving, subsurface grains from τ'''. For a flat bed, form drag is absent, so that $\tau' + \tau''' = \tau$. For sheet flow conditions, the τ''' component is generally considered to be the dominant component.

In the present paper, it is first assumed that sediment conditions are such that bed forms do not form so that the bed can be considered flat. The sheet flow model, in which the dominant shear stress is taken to be τ''', is used with a fixed value of the δ_{sx}/δ_n ratio of 0.5 as suggested by earlier sheet flow work (Kaczmarek et al. 1994), to determine the thickness of the bedload layer and sediment transport rate for a range of sediment conditions covering both low and high wave conditions. Comparison of sediment transport rates and bedload layer thicknesses is then made with a number of data sets, including those of Sawamoto & Yamashita (1986), as reported by Nielsen (1992); with small-scale laboratory tests conducted at IBW PAN, Gdańsk, Poland; with oscillating tunnel data of Ribberink & Al-Salem, as reported by Van Rijn (1993); and with flume data of Sumer et al. (1996). Next, comparison is made between the effective roughness of the sediment boundary produced by the model and experimental data reported by Nielsen (1992). The results for flat bed conditions at low wave conditions suggest that the ratio δ_{sx}/δ_n varies with wave conditions. Comparison of sediment transport rates from the model with variable δ_{sx}/δ_n values with Sawamoto & Yamashita's data, as well as limited data from IBW PAN tests, is then made to show that the model yields reasonable values. Finally, the sheet flow model with $\delta_{sx}/\delta_n = 0.50$ is applied to Ribberink & Al-Salem sheet flow data to show that it yields good values for sediment concentration during the wave period.

2. Theory

2.1. Formulation of the Problem

The velocity profile in the transition zone is assumed to be continuous. Its intersection with the nominal seabed is the apparent slip velocity u_b. The downward extension of the velocity distribution in the outer zone of the main flow yields a fictitious slip velocity u_0 at the nominal static bed level.

The velocity distribution around a flat porous rough bed is controlled by bed roughness and bed permeability. For the present, it is assumed that the velocity is determined by roughness geometry and outer flow parameters, such as the free-stream wave velocity.

The procedure described below permits matching of velocities in regions I and II. The velocity profile in the upper turbulent layer, which is linked with identification of an effective bed roughness height, k_e, is determined first, and

then passed to the lower collision-dominated layer. The intersection of the two velocity profiles is marked as point A in Figure 1.

2.2. Flow in the Turbulent Upper Region

It is assumed that the flow in the upper layer is described by the logarithmic distribution:

$$\frac{u}{u_f} = \frac{1}{\kappa} \ln \frac{30y}{k_e} \tag{1}$$

in which u_f and κ are the effective flow shear velocity and the von Karman constant (equal to 0.4), respectively and k_e is the effective roughness height related to the location of the fictitious point of zero velocity of the outer flow.

In this work use is made of the value $u_{f\,\max}$ which is the maximum bed shear velocity ($u_f(\omega t)$) during the wave period $T = 2\pi/\omega$, that is $\max[u_f(\omega t)]$.

The quantity $u_{f\,\max}$ is determined from the solution of the integral momentum equation for wave boundary layer flow derived by Fredsøe (1984):

$$\frac{\tau(\delta)}{\rho} - \frac{\tau_0}{\rho} = -\int_{\frac{k_e}{30}}^{\delta+\frac{k_e}{30}} \frac{\partial}{\partial t}(U-u)dy \tag{2}$$

in which δ is the wave boundary layer thickness; it being assumed that all the applied hydrodynamic stress is balanced by the internal resistance from the collision-dominated bedload layer.

The boundary condition at the upper limit of the boundary layer is taken as $u = U$ at $y = \delta + k_e/30$, where U is the free stream velocity. On the basis of Equation (1), it is possible to write:

$$\delta = \frac{k_e}{30}\left(e^{z_1} - 1\right) \tag{3}$$

in which

$$z_1 = \frac{U\kappa}{u_f} \tag{4}$$

Fredsøe (1984) obtained a differential equation for the variation of z_1 after re-arranging the integral on the right side of Equation (2), thus providing the equation:

$$\frac{dz_1}{d(\omega t)} = \frac{30\kappa^2 U(\omega t)}{k_e \omega e^{z_1}(z_1 - 1) + 1} - \frac{z_1(e^{z_1} - z_1 - 1)}{e^{z_1}(z_1 - 1) + 1} \frac{1}{U} \frac{dU}{d\omega t}. \tag{5}$$

The solution of Equation (5) has been achieved in the present study by the Runge-Kutta second-order method. As a result, the function $z_1(t)$ has been obtained and the temporal distributions of the boundary layer thickness $\delta(t)$ and the friction velocity $u_f(t)$ are given by Equations (3) and (4), respectively. The

solution of Equation (5) yields the value of $u_{f\max}$ if k_e is specified as a fixed, constant value.

2.3. Effective Stresses and Flow in the Collision-Dominated Granular-Fluid Region

The sub-bed flow (subzone I) is described within an (x', z') co-ordinate system in which x' is a horizontal axis and z' is a vertical axis, with the origin at the theoretical bed level, see Figure 1. The sediment in this subzone is carried by the intergranular stresses and its weight is transferred to the soil skeleton in the immobile bed. It is assumed that at any given level the sediment and water move with the same velocity. The following equations, which indicate equilibrium of horizontal and vertical forces, can be used to describe conditions in the steady water-soil mixture flow, as proposed by Kaczmarek (1991):

$$\frac{\partial \sigma_{x'z'}}{\partial z'} = 0 \tag{6}$$

$$c(\rho_s - \rho)g + \frac{\partial}{\partial z'}(\sigma_{z'z'}) = 0 \tag{7}$$

where ρ_s and ρ are the grain and water density, respectively.

Particle interactions in the sheet flow layer are assumed to produce two distinct types of behaviour. Coulomb friction between particles gives rise to rate-independent stresses (of the plastic type) and the particle collisions give rise to stresses that are rate-dependent (of the viscous type). Furthermore, we assume the co-existence of both types of behaviour in the regime of flow considered here. Accordingly, the effective stress tensor is divided into two parts, see Sayed & Savage (1983)

$$\sigma_{ij} = \sigma_{ij}^0 + \sigma_{ij}^* \tag{8}$$

where σ_{ij}^0 is the plastic stress and σ_{ij}^* the viscous stress. The tensile normal stresses are considered positive.

In order to describe the dynamic stresses, use is made of Sayed & Savage's (1983) suggestions for the description of the viscous stresses due to chaotic grain collisions, and for plastic stresses. Thus, for the case of a simple shear flow, it is possible to write the following equations for the normal and viscous shear stresses:

$$\sigma_{x'x'}^* = \sigma_{z'z'}^* = -(\mu_0 + \mu_2)\left(\frac{\partial u}{\partial z'}\right)^2 \tag{9}$$

$$\sigma_{x'z'}^* = \sigma_{z'x'}^* = \mu_1 \left|\frac{\partial u}{\partial z'}\right| \frac{\partial u}{\partial z'} \tag{10}$$

where $\sigma_{x'x'}^* = \sigma_{z'z'}^*$, $\sigma_{x'z'}^* = \sigma_{z'x'}^*$ are the normal and shear stresses, respectively.

The coefficients μ_0, μ_1 and μ_2 are functions of the solids concentration c and may be estimated on the basis of the relationships proposed by Sayed & Savage (1983),

$$\frac{\mu_1}{\rho_s d^2} = \frac{0.03}{(c_m - c)^{1.5}} \tag{11}$$

$$\frac{\mu_0 + \mu_2}{\rho_s d^2} = \frac{0.02}{(c_m - c)^{1.75}}. \tag{12}$$

In the above equations d is the diameter of the solid particles and c_m (equalled to 0.53) is the solid concentration corresponding to a stationary, closely packed bed. Thus, the particle collisions give rise to non-Newtonian stresses that are proportional to the square of the velocity gradient and increase rapidly with increasing concentration of solids.

For two-dimensional deformation in the rectangular Cartesian co-ordinates x' and z', the Mohr-Coulomb yield criterion is satisfied by employing the following stress relations for plastic stresses:

$$\sigma^0_{x'x'} = -\sigma'(1 + \sin\varphi \cos 2\psi) \tag{13}$$

$$\sigma^0_{z'z'} = -\sigma'(1 - \sin\varphi \cos 2\psi) \tag{14}$$

$$\sigma^0_{x'z'} = -\sigma' \sin\varphi \sin 2\psi \tag{15}$$

where φ is the quasi-static angle of internal friction, ψ is the angle between the major principal stress and the x'-axis, and σ' is the average normal stress:

$$\sigma' = -\left(\frac{\sigma^0_{x'x'} + \sigma^0_{z'z'}}{2}\right). \tag{16}$$

For isothermal flow, the stress σ' depends only on the bulk density, or in the case of incompressible grains, the concentration of solids c. Here the following approximate expression proposed by Sayed & Savage (1983) is used:

$$\sigma' = \alpha^0 \left(\frac{c - c_0}{c_m - c}\right) \tag{17}$$

in which α^0 is a constant which may be assumed to have the following form:

$$\frac{\alpha^0}{\rho_s g d} = 1 \tag{18}$$

where g is the gravitational acceleration and c_0 the solid concentration (equal to 0.32) corresponding to bed fluidisation and to a state of zero residual shear resistance.

For simple shear flow, the angle between the major principal stress and the x' axis is equal to (Sayed and Savage 1983):

$$\psi = \frac{\pi}{4} - \frac{\varphi}{2}. \tag{19}$$

The continuity of the shear stress at the theoretical bed level requires:

$$\rho u_f^2 = \mu_1|_{c=c_0} \left(\frac{\partial u}{\partial z'}\right)^2\Bigg|_{z'=0}. \tag{20}$$

Using Equations (9), (10) and (13), (14), (15) the balance of linear momentum (6) and (7), according to Kaczmarek (1991) yields:

$$\alpha^0 \left(\frac{c - c_0}{c_m - c}\right) \sin\varphi \sin 2\psi + \mu_1 \left(\frac{\partial u}{\partial z'}\right)^2 = \rho u_f^2 \tag{21}$$

$$\alpha^0 \left(\frac{c - c_0}{c_m - c}\right)(1 - \sin\varphi \sin 2\psi) + (\mu_0 + \mu_2)\left(\frac{\partial u}{\partial z'}\right)^2 =$$

$$= \left(\frac{\mu_0 + \mu_2}{\mu_1}\right)\Bigg|_{c=c_0} \rho u_f^2 + (\rho_s - \rho) g \int_0^{z'} c\,dz' \tag{22}$$

By eliminating $\left(\frac{\partial u}{\partial z'}\right)^2$ from Equations (21) and (22) one obtains at level z':

$$\alpha^0 \left(\frac{c - c_0}{c_m - c}\right)\left[1 - \sin\varphi \sin 2\psi - \left(\frac{\mu_0 + \mu_2}{\mu_1}\right)\sin\varphi \sin 2\psi\right] =$$

$$= \rho u_f^2 \left\{\left[\frac{\mu_0 + \mu_2}{\mu_1}\right]_{c=c_0} - \left[\frac{\mu_0 + \mu_2}{\mu_1}\right]\right\} + (\rho_s - \rho) g \int_0^{z'} c\,dz' \tag{23}$$

The system of Equations (21) and (22) enables the calculation of the vertical profiles of the sub-bed sediment concentration c and velocity u in relation to a known shear stress (ρu_f^2) at the theoretical bed level ($z' = 0$) for the various bed material characterised by values φ, d and ρ_s and for fixed values of c_0 and c_m.

3. Computations

3.1. Computational Background

Equation (23) can be solved for c as a function of z' by an iteration method in conjunction with numerical integration. Integration starts at the theoretical bed level ($z' = 0$) with $c = c_0$. Proceeding downwards at each step, an initial estimated

value is used in Equation (23) to evaluate c. The calculated value of c is next used to obtain a better estimate of c. Iteration is stopped when the change in the value of c becomes negligible. Convergence is found to occur rapidly. The numerical integration was carried out using the trapezoidal rule.

It is also necessary to assume the maximum value of c at which the bed would shear freely. In the present study, the maximum c value for shear, c_{ms} has been taken as 0.5, after Sayed & Savage (1983), hence the denominators in Equations (21)–(23) are never zero. For concentrations exceeding 0.5 it is assumed that the particles are locked together as a rigid mass. Integration is stopped when c equals c_{ms}. This level is denoted as δ_n.

The values of c are then used to calculate the velocity u from Equation (21), Integration starts at the level δ_n where $c = c_{ms}$ with $u = 0$. At each computational level z', the value of u is checked so as to ensure that the computation does not result in negative values (cf. the form of Eq. (21)), In such cases the computed velocities are replaced by zeros. The last singular point is denoted as the ordinate δ_s, thus indicating the zero velocity level . The calculations are carried out thereafter towards the theoretical bed level $z' = 0$.

In the present model of the sub-bed flow, the plastic stresses disappear at the theoretical bed level and the viscous stresses described by the relationships (9) and (10) are in agreement with the sheet flow description proposed by Engelund & Fredsøe (1976). The latter authors used Bagnold's concept for the stresses due to particle-particle interactions (called dispersive shear stresses), which were taken as proportional to the squared velocity gradient with the coefficient related to the volume concentration. By employing Bagnold's ideas as to how the fluid shear stress is transferred to a bed covered by loose sediment, Engelund & Fredsøe (1976) found a functional relationship between the bed concentration c_b at a distance of the order of two grain diameters from the bed, together with the bed shear stress. Values of c_b become extremely small for very small and approach 0.32 for large values of bed shear stress.

3.2. Procedure

The theoretical bed level is defined by the matching point of the velocity distribution in the turbulent region and the sub-bed flow profile (Fig. 1). The matching point is assumed to take place at the phase of maximum shear stress, although at any other phase of oscillatory motion there must be some transition between the two profiles. Both velocity profiles depend on k_e, which is not known a priori. Upon selection of a certain initial value for k_e, the iterative computations are continued as long as the sub-bed and logarithmic velocity profiles coincide at the $y = \delta_{sx} + k_e/30$ level. The quantity δ_{sx} , being taken as a certain fraction of δ_n, is shown in Figure 1 as a limit of the downward extension of the turbulent velocity distribution from matching point A.

An iteration procedure is proposed for finding the matching point between the turbulent and sub-bed velocity profiles. The turbulent profile is found from Equation (1) for the wave phase of the maximum shear stress $\rho u_{f\,\max}^2$, which is calculated from Equation (5) while the system of Equations (21) and (22) provides the value δ_{sx} and the sub-bed velocity profile in relation to the known maximum shear stress ($\rho u_{f\,\max}^2$), The calculations are stopped when the velocity at the top of the sub-bed layer attains the value determined from Equation (1) at $y = \delta_{sx} + k_e/30$.

4. Experimental Evidence

The value of δ_n is determined from Equations (21) and (22) for maximum shear stress. The selection criterion for δ_{sx} (which is a certain fraction of δ_n) can be based on the degree of fit to experimental data comprising bedload thickness and transport rate. A value of $\delta_{sx} = 0.5\delta_n$ is shown below to be a reasonable assumption for sheet flow conditions.

The computational procedure described above was previously run by Kaczmarek & O'Connor (1993a, b) for the following conditions of Horikawa's et al. (1982) Test I: $d = 0.2$ mm, $s = 2.66$, $\varphi = 24.4°$, $T = 3.6$ s, $U_{1m} = 127$ cm/s. The quantity δ_{sx}/δ_n was taken as 0.50 and the effective roughness was found to be $k_e = 7.3$ mm. Kaczmarek & O'Connor (1993a, b) used the procedure outlined above to find k_e. However, the turbulent profile for the wave phase of maximum shear stress was found from a numerical solution of the momentum equation for the wave boundary layer (proposed by Kaczmarek & Ostrowski (1992) with Brevik's (1981) type of eddy viscosity) instead of using the simpler Equation (1). Knowing k_e the instantaneous velocity profiles were obtained from Equations (21) and (22), and numerical solution of the turbulent boundary layer flow. The results of computations were presented by Kaczmarek et al. (1994) against experimental data and conformity was found to be satisfactory for the sheet flow regime.

Knowing k_e from the iteration procedure with $\delta_{sx} = 0.5\delta_n$, it is possible to calculate from Equations (21) and (22) both the instantaneous sediment velocity and concentration distributions in the *bedload layer*, as well as the instantaneous bedload thickness δ_s. Following Nielsen (1992), the vertical scale of the bedload distribution can be defined as:

$$L_B = \frac{1}{0.63} \int_0^{\delta_s} c(z')dz' \tag{24}$$

The results of computations with $\delta_{sx} = \delta_n/2$ are shown in Figure 2a while the comparison of these results with the measurements of Sawamoto & Yamashita (1986), as presented by Nielsen (1992), is shown in Figure 2b. The calculations were carried out for the maximum shear stress occurring during the wave period

and for a variety of wave and sedimentological conditions including those of Sawamoto & Yamashita (1986), i.e. quartz sand with $d = 0.2$ mm and 0.7 mm, for 8 wave data sets (cf. Tables 1 and 2 in Sawamoto & Yamashita (1986)). The agreement of both the general trend and the numerical values is good for large $\theta_{2.5}$ values corresponding to sheet flow conditions, but not so good for low wave conditions. The quantity $L_{B,\max}$ resulting from the iteration procedure is presented as a function of $\theta_{2.5}$ defined by the equation:

$$\theta_{2.5} = \frac{1}{2} f_{2.5} \psi_1 = \frac{1}{2} f_{2.5} \frac{(a_{1m}\omega)^2}{(s-1)gd} \tag{25}$$

where $s = \rho_s/\rho$ is the relative sediment density, in order to compare other authors' findings with those given here. The special grain roughness friction factor $f_{2.5}$ is based on a roughness $2.5d_{50}$, where d_{50} is a median grain size using the equation, Nielsen (1992):

$$f_{2.5} = \exp\left[5.213\left(\frac{2.5d_{50}}{a_{1m}}\right)^{0.194} - 5.977\right]. \tag{26}$$

Further model comparisons have been made using the oscillating tunnel experimental data of Ribberink & Al-Salem (1992), presented by Van Rijn (1993). Here, the time-averaged load L_t was defined as the integration over the depth of the time-averaged concentrations. Figure 2c shows the load L_t as a function of the peak forward orbital velocity from the oscillating tunnel data in comparison with the present model. The model results for almost all tests lie below the measured data. However, it should be noted that the present theory concerns only bedload transport while the experiments of Ribberink and Al-Salem comprise a relatively wide range of hydrodynamic conditions under which both bedload and suspended load are present.

Further information is provided by Sumer et al. (1996) who define δ_s as the thickness of the sheet-flow layer. The value δ_s has been measured by visual observations, and hence may be subject to some degree of uncertainty. Figure 3 shows the comparison of the present model values of $\delta_{s,\max}$ (i.e. δ_s for maximum shear stress during the wave period) with Sumer et al. (1992) data presented in terms of the quantity $\theta_{\max}(2.5d)$. The value $u_{f\max}(2.5d)$ in $\theta_{\max}(2.5d)$ originates from Fredsøe's model (Eq. (5)) for a roughness of $2.5d_{50}$, instead of the original u_f in θ taken from fitting the measured velocity distributions to logarithmic profiles. This stems from two reasons: (1) the bedload thickness depends on $\theta_{2.5}$, as shown in Figure 2a; (2) Sumer et al. (1996) show that the roughness maintains its usual value ($2.5d$) for the range of $\theta < 1.5$. A good model fit is obtained around $\theta_{2.5} \approx 1$ but discrepancies exist at both lower and higher values. Discrepancies at high $\theta_{2.5}$ values may be due to the neglect of suspended load in the present model.

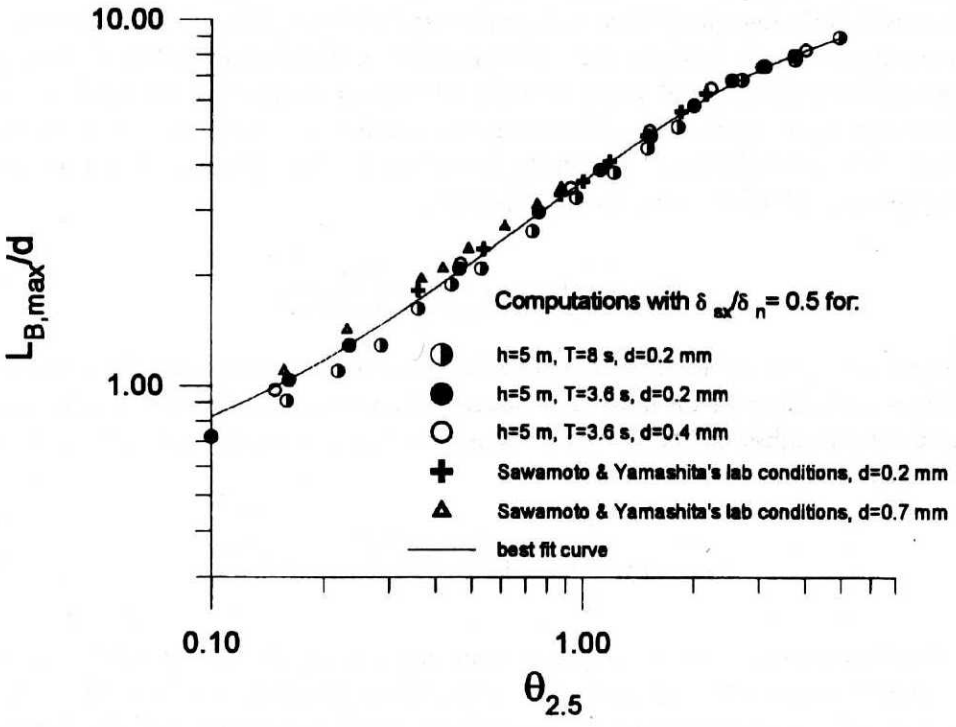

Fig. 2a. Model bedload thickness $L_{B,\max}$ with $\delta_{sx}/\delta_n = 0.5$

On the basis of the above tests and comparisons with experimental data, it is concluded that $\delta_{sx} = \delta_n/2$ is a realistic assumption to use for bedload in sheet flow conditions. A similar conclusion is obtained from the calculations of bedload rate, defined as follows:

$$Q_B = \int_0^{\delta_s} u(z', t)c(z', t)dz' \tag{27}$$

The instantaneous transport rate Q_B is computed from Equation (27) by the iteration procedure for k_e, from which the instantaneous sediment velocity $u(z', t)$ and concentration $c(z', t)$ distributions in the bedload layer are obtained, and by use of Equations (21) and (22) in relation to the instantaneous shear stress known from Equation (5), A dimensionless flux ϕ_B is then defined by the equation:

$$\phi_B = \frac{Q_B}{d\sqrt{(s-1)gd}}. \tag{28}$$

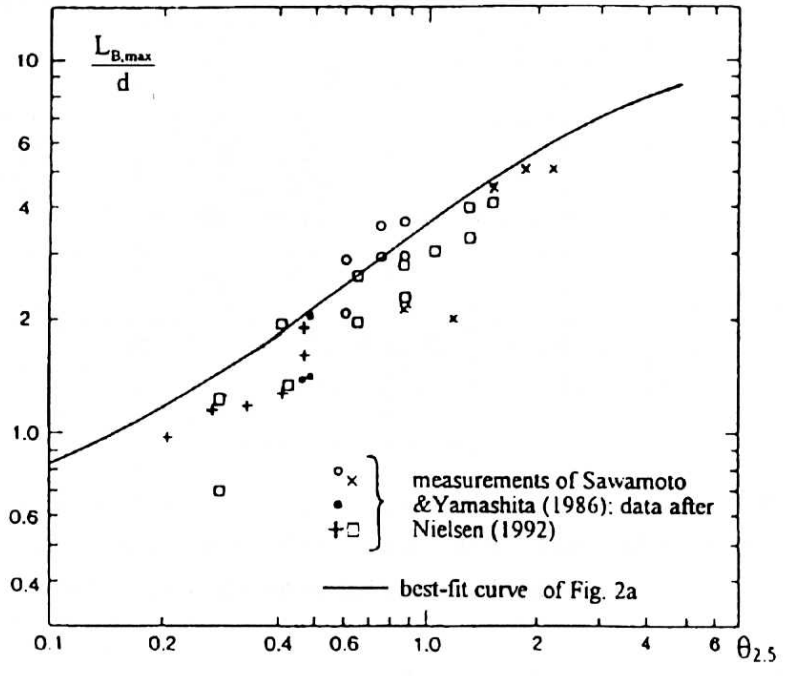

Fig. 2b. Model bedload thickness $L_{B,\max}$ (with $\delta_{sx}/\delta_n = 0.5$) vs. laboratory measurements of Sawamoto & Yamashita, data after Nielsen (1992)

Figure 4a shows the results of the computations of ϕ_B for maximum shear stress conditions during the wave period for various conditions covering a wide range of $\theta_{2.5}$. The transport rate can be approximated by the curve:

$$\phi_{B\max} = 3.4\theta_{2.5}^{1.5} \tag{29}$$

while the approximation of theoretical results averaged over $T/2$ yields:

$$\phi_{T/2} = 1.3\theta_{2.5}^{1.5}. \tag{30}$$

The comparison of the calculated dimensionless bedload rate averaged over half a wave period ($T/2$), given as a solid line, with the laboratory data of Sawamoto & Yamashita and Horikawa et al., as presented by Nielsen (1992), is shown in Figure 4b. Conformity is considered to be good, except for the data for large $\phi_{T/2}$ values, which correspond to data for fine sand, where suspended load is significant. Figure 4b also includes data from laboratory studies at IBW PAN, which are discussed in the next section.

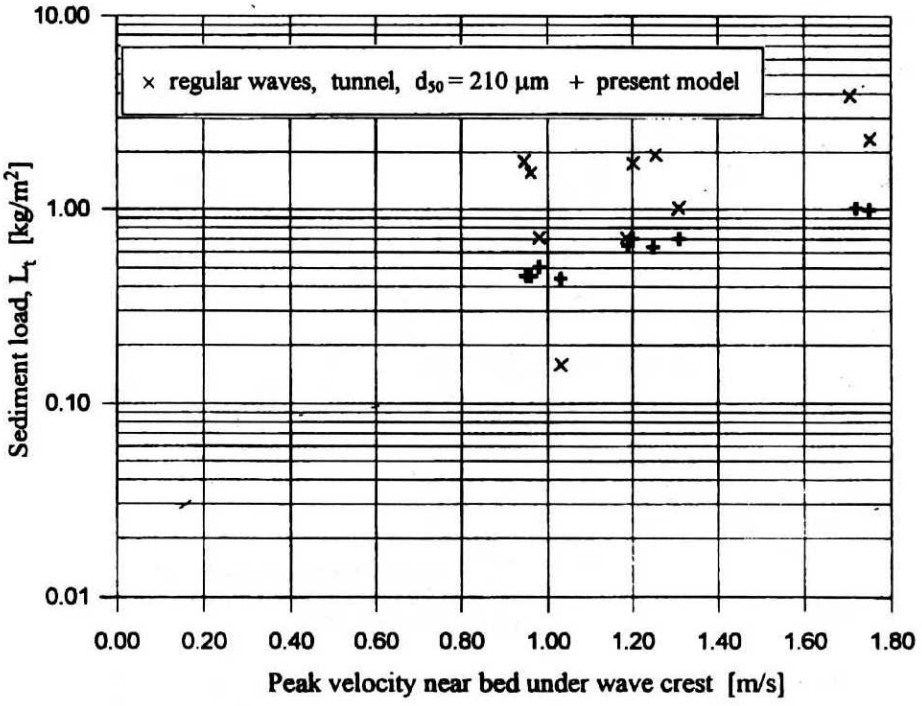

Fig. 2c. Model time-averaged sediment load L_t vs. laboratory measurements of Ribberink and Al-Salem, experimental data after Van Rijn (1993)

5. Experimental Analysis of Bedload Transport

5.1. Experimental Setup and Procedure

The bedload sediment transport measurements were carried out in the IBW PAN wave flume for a range of regular and random wave tests with a single sediment size. The wave flume, 0.5 m wide and 22.5 m long, can use water depths of up to 0.7 m. Reinforced concrete slabs 8 cm thick were placed on the bottom to contain a sandy measuring section (also 8 cm thick) 7 m in length centred about the middle of the flume. Natural sand with a grain diameter of $d_{50} = 0.22$ mm was used in the experiments and a 6.3 cm deep sand trap was located within the sandy section 2 m from its end.

For each test, free surface elevation was measured at three points along the flume. The horizontal component of free stream velocity was measured at one point in the measuring section, using a micro-propeller, together with one of the wave gauges, which was located above a sand trap. The other two wave gauges were spaced $1/4^*L$ from each other (L being a wave length) to estimate reflection effects which were found to be generally small, (in the flume 10-20% of incident

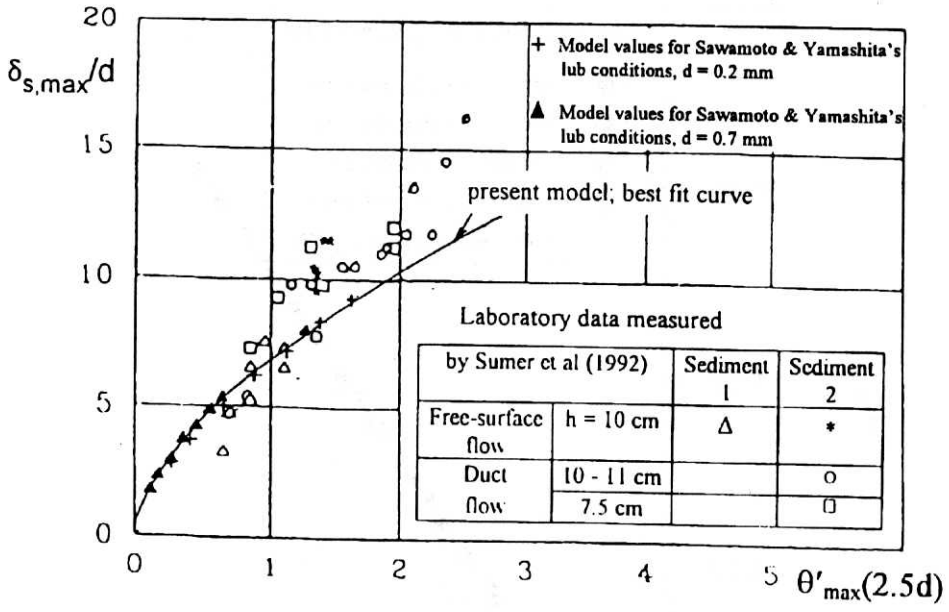

Fig. 3. Model bedload transport thickness $\delta_{s,max}$ vs. laboratory data of Sumer et al. (1996)

wave heights).The experimental setup, together with the sand trap, is shown in Figure 5.

The sand trap, which consisted of two cells to measure both onshore and offshore bedload components, was covered by a lid and buried in the sandy section before each test. Waves were then generated until bed ripples were fully formed, which took some 25-60 minutes. The lid, suspended on four strings, was removed thereafter, together with the thin layer of sand on it. The wave action was then continued for a further 1.2–15 minutes during which time sediment grains were caught in the sand trap. Finally, the grains were siphoned from the trap and weighed to determine the sedimentation quantity. The geometrical properties of the bed forms were also measured so that their shape was known after each test.

A constant water depth of $h = 0.5$ m was maintained in the measuring section during each test. The experiments were repeated many times for each set of wave parameters. In all, 141 tests were run, including 103 with mono-frequency waves (represented by Tests 1, 2, 3, 4, 11 and 12) which have been analysed in the present paper.

The conditions expressed in terms of $\theta_{2.5}$ varied roughly from 0.1 in Test 3 to 0.4 in Test 12. This range of rippled bed (cf. Fig. 4b) is extremely important as the majority of the transport occurs as bedload in this regime since suspended load is small. At higher flow rates bedload will play only a minor role.

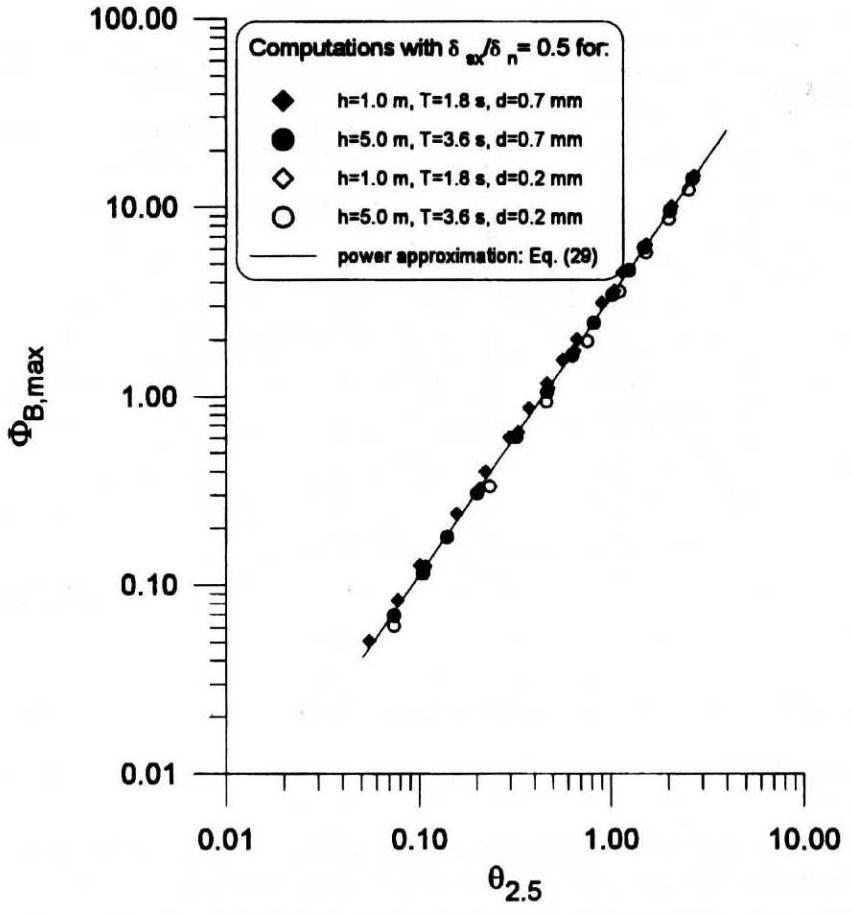

Fig. 4a. Model bedload transport rate for maximum effective shear stress during the wave period

5.2. Model results vs. IBW PAN Laboratory Measurements

The experimental results are shown in Figure 6 and are compared with bedload data obtained from Equation (30).

The waves measured in the flume were found to be slightly asymmetric in shape, therefore, for better representation of actual laboratory conditions, the theoretical results have been re-worked using the present model operated with non-linear waves. The free stream velocity in Equation (5) was described using 2nd order Stokes theory, as indicated by Kaczmarek & Ostrowski (1992). Then, for known distributions of u_f in time, the instantaneous bedload transport rate was found from Equations (21) and (22) for the entire wave period, integrated over time and averaged over the wave period. The results are also shown in Figure 6.

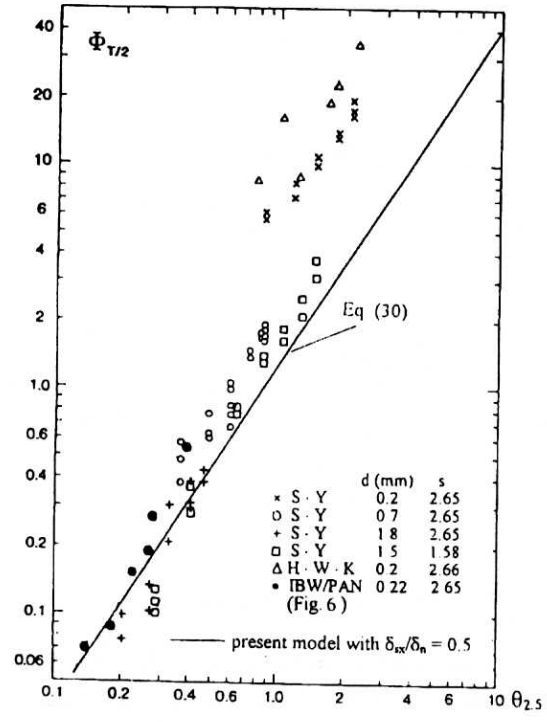

Fig. 4b. Model bedload rate vs. laboratory data of Sawamoto & Yamashita, Horikawa et al. (as given by Nielsen (1992)) and IBW PAN laboratory data

A reasonable comparison of model and experimental data can be seen in Figure 6, especially using the non-linear wave approach (except for Test 2). It should be pointed out that for long and highly asymmetric waves, represented by Test 11 (Ursell parameter of 40), the experimental data fits the non-linear model much better than the linear model. The largest shear stress conditions generated in the flume without wave breaking had a value of $\theta_{2.5} = 0.4$ and were achieved in Test 12. However, the Ursell number (equalled to 31) was less than in Test 11. In Test 12, a very distinct concentration of suspended sediment was observed which resulted in increased accumulation in the sand trap so that the experimental result is larger than the model values, using either linear or non-linear wave theory.

6. Comparison of the Effective and Apparent Roughnesses

Conformity between the laboratory data for bedload sediment transport rate and that calculated by the present theory with $\delta_{sx}/\delta_n = 0.5$ was found to be good for low θ which denotes a rippled bed. The present approach makes use of a single fitting constant to enable the upper and lower layer velocity profiles to be matched

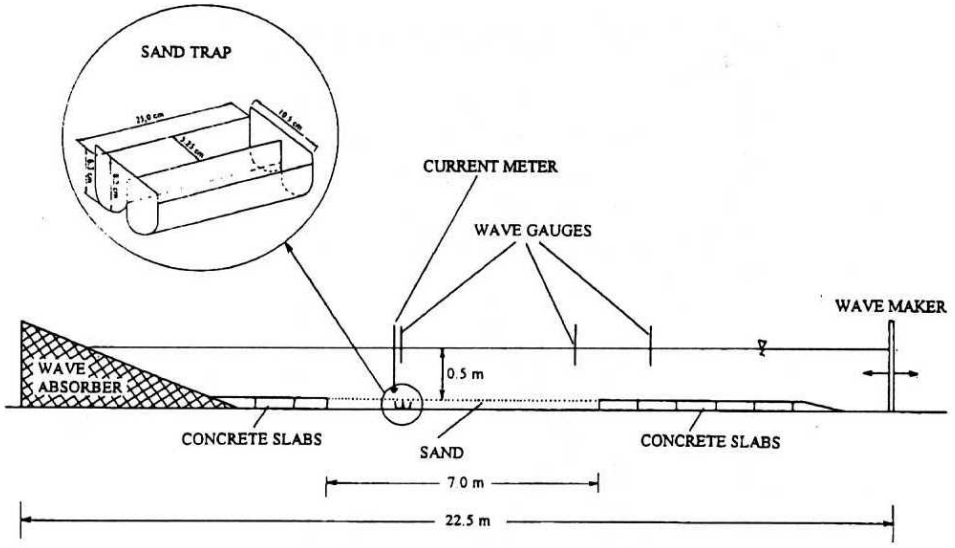

Fig. 5. IBW PAN experimental setup

at theoretical point A (Fig. 1), The fitting constant (k_e) is taken at the level of zero velocity of the outer layer logarithmic velocity profile and as such could be interpreted as the effective roughness height of the bed, in terms of the outer flow.

The present model was next run for a wide range of small ($h = 1.0$ m, $T = 1.8$ s) and large scale ($h = 5.0$ m, $T = 3.6$ s) conditions and for two diameters of sandy bed. The results of computations obtained by use of the iteration procedure are shown in Figure 7a in terms of the grain friction parameter $\theta_{2.5}$ defined by Equations (25) and (26), The model findings can be represented by the curve:

$$\frac{k_e}{d} = 47\theta_{2.5}^{-0.658}. \tag{31}$$

The trend shown in the present results, i.e., that the effective roughness height increases with decreasing $\theta_{2.5}$, is similar to that shown by Nielsen (1992) for an apparent roughness corresponding to rippled beds, found from available friction and energy dissipation data (Fig. 7b). Nielsen (1992) showed that the apparent roughness for equilibrium ripple formations is of the order $100d$ to $1000d$ and arises from the external form drag produced by bed forms, which is not included in the present paper. For artificial flat beds where measurements were taken before ripples had time to form, Nielsen (1992) suggested that the apparent roughness decreased with decreasing grain roughness Shields parameter. In terms of grain roughness Shields parameter $\theta_{2.5}$, the roughness corresponding to total drag on a

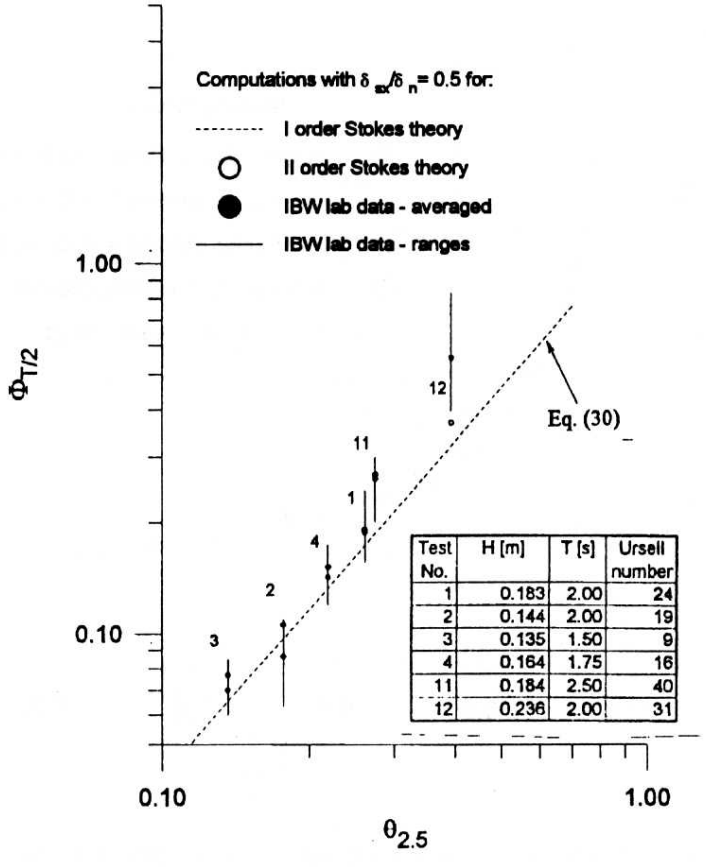

Fig. 6. Bedload laboratory data (IBW PAN) vs. present model results

flat sand bed in the ripple regime may be expressed by the equation:

$$\frac{k_a}{d} = 170\sqrt{\theta_{2.5} - \theta_c} \tag{32}$$

see Figure 7b. In Eq. (32) θ_c denotes the critical Shields parameter at which sediment movement starts (≈ 0.05).

Because the form drag is absent in the case of artificial flat beds, it is assumed that the total drag is applied to the sediment load. In order to investigate this aspect, a series of sensitivity tests on the variation of k_e with the ratio δ_{sx}/δ_n has been performed. Initially, three values of a constant ratio of $\delta_{sx}/\delta_n (= 0.1, 0.5, 0.9)$ were used. The results are illustrated in Figure 8a. It can be seen that the trends of the k_e curves are identical for all ratios of δ_{sx}/δ_n. This trend is, however, related to the constant value of δ_{sx}/δ_n ratio kept for the entire range of $\delta_{2.5}$. Using Equation (32), it is possible to determine the variation of δ_{sx}/δ_n with $\delta_{2.5}$ so that the model reproduces the observed variation in k_a, see Figure 8b.

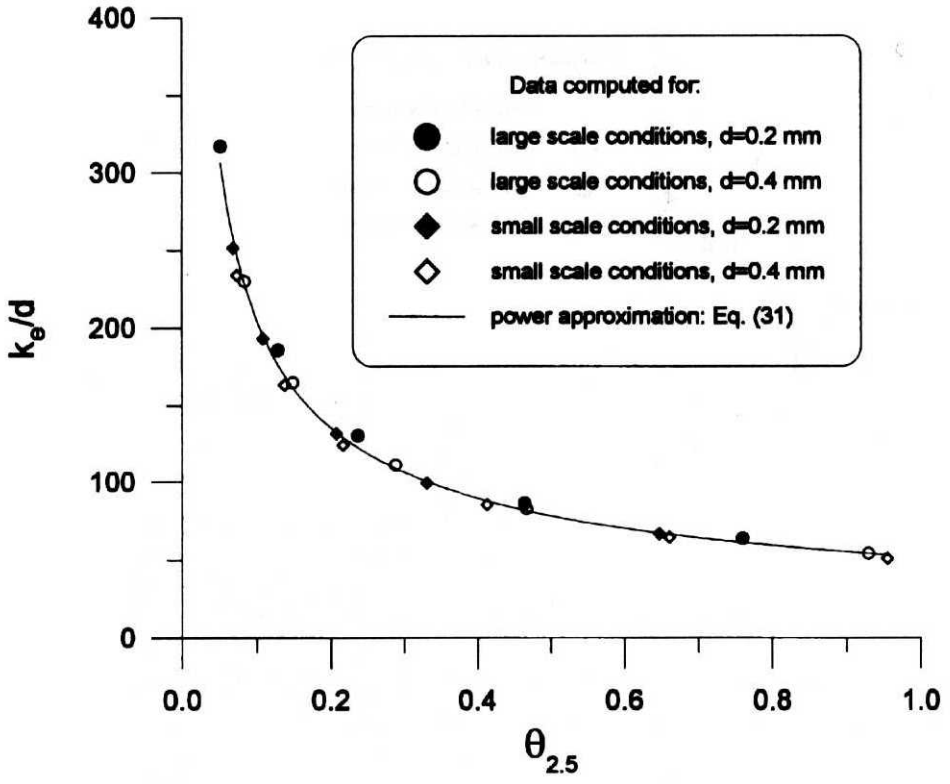

Fig. 7a. Results of effective bed roughness computations with $\delta_{sx}/\delta_n = 0.5$

Next, using the variable δ_{sx}/δ_n values, calculations were made using Equations (21) and (22) to find bedload properties such as bedload thickness and transport rate. These calculations have been carried out for a wide range of wave heights and for two sets of depth and period values, i.e. $h = 5$ m, $T = 3.6$ s and $h = 10$ m, $T = 8.39$ s, with $d = 0.2$ mm for both sets of parameters and additionally $d = 0.7$ mm for the long-period data set.

The results of computations shown in Figures 9a and 9b reveal that the present approach with the fitting parameter k_e given by Eq. (32) provides a good approximation of bedload thickness for (artificially) flat beds at low flow intensities ($\theta_{2.5} \leq 0.4$), In the range of relative effective roughness values with $\theta_{2.5} \geq 0.4$ the theoretical results overestimate the experimental data. It seems that, for this range of $\theta_{2.5}$, the present approach with the fitting parameter k_e given by Equation (31), i.e. with constant ratio $\delta_{sx}/\delta_n = 0.5$, provides a better estimation of bedload thickness.

The same conclusions can be reached from Figures 10a and 10b where the calculations of bedload rate are shown for both fixed and variable values of δ_{sx}/δ_n

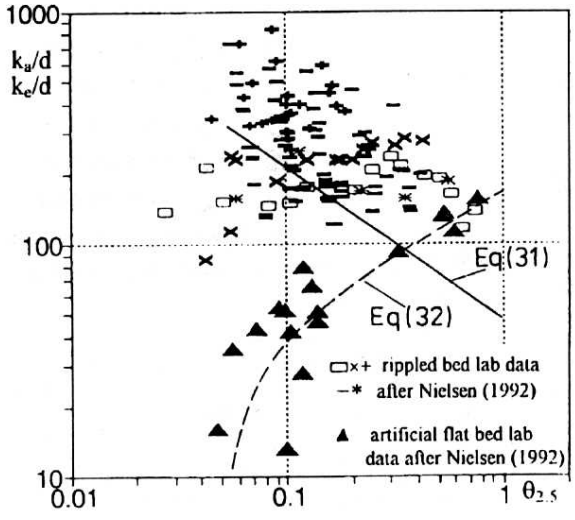

Fig. 7b. Comparison of an apparent roughness found from friction and dissipation laboratory data (k_a) with computed effective roughness (k_e) for $\delta_{sx}/\delta_n = 0.5$ (solid line) and for variable δ_{sx}/δ_n (dashed line)

ratio. In addition, the model results are compared with those from a special IBW PAN experimental test, corresponding to those of Test 2 for rippled bed conditions, in which the bed was artificially smoothed to maintain the conditions of a flat bed. The experimental results for bedload rate for an artificial flat bed are compared in Figure 10a with the results obtained in the presence of ripples.

It seems that the present model is capable of reproducing the hydrodynamic drag and sediment transport rate on flat beds of sediment for both low and high wave conditions provided the model is operated with variable δ_{sx}/δ_n values with a magnitude less than or equal to 0.50. If the model is used with a fixed ratio of $\delta_{sx}/\delta_n = 0.50$, it is possible via Equation (31) to reproduce realistic estimates for total drag corresponding to rippled conditions although form drag is not explicitly included in the model. The realistic nature of Equation (31) is further demonstrated by calculation of wave-friction factor f_w, using Jonsson & Carlsen's (1976) formula for conditions appropriate to Madsen et al.'s (1990) laboratory tests for regular waves. The results shown in Fig. 11 are presented in terms of a representative value of a fluid-sediment interaction parameter, defined by Madsen et al. (1990) as:

$$S_r = \frac{\theta_{\max}(d)}{\theta_c} \tag{33}$$

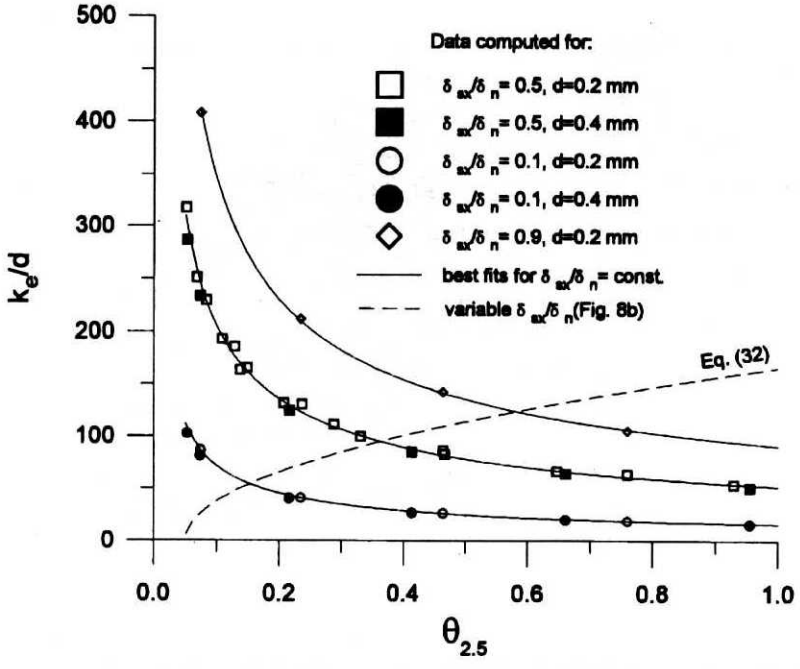

Fig. 8a. Results of sensitivity tests with δ_{sx}/δ_n for effective bed roughness

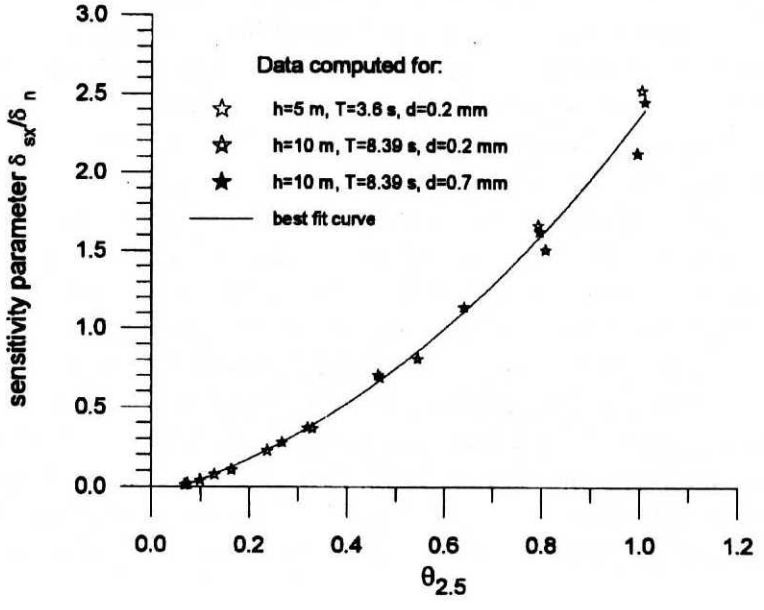

Fig. 8b. Variation of sensitivity parameter δ_{sx}/δ_n with $\theta_{2.5}$

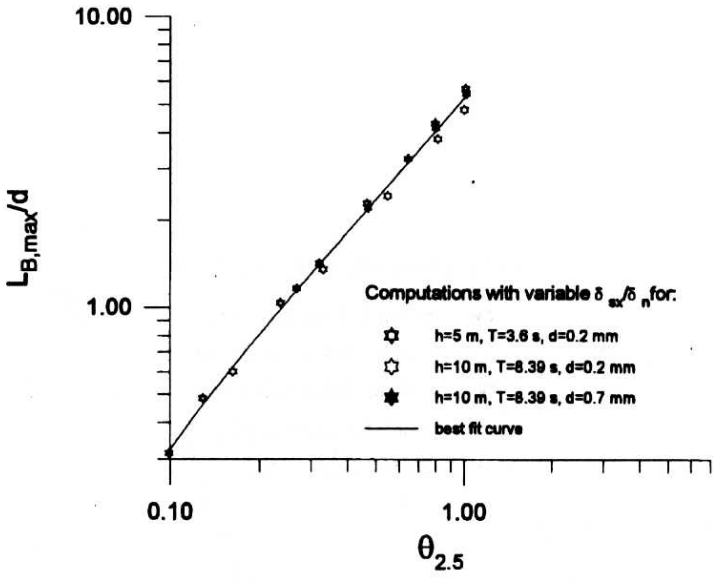

Fig. 9a. Model bedload thickness $L_{B,\max}$ with variable δ_{sx}/δ_n

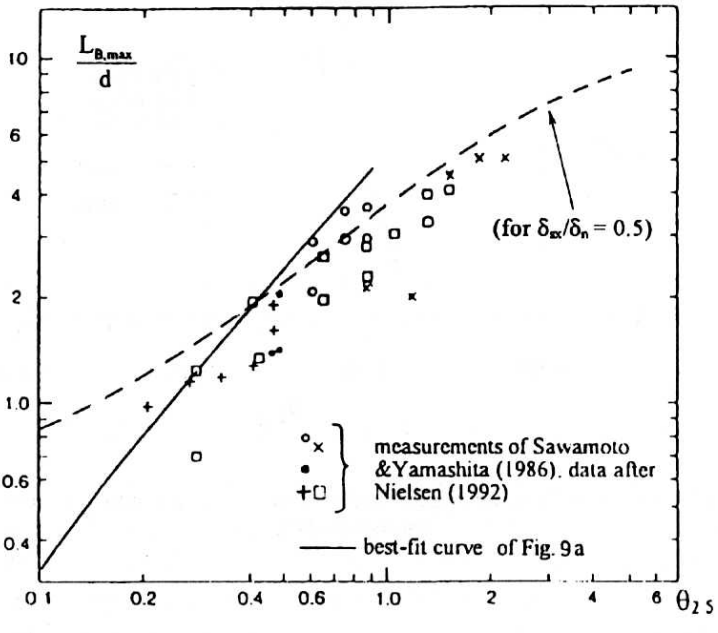

Fig. 9b. Model bedload thickness $L_{B,\max}$ (with variable δ_{sx}/δ_n) vs. laboratory measurements of Sawamoto & Yamashita, data after Nielsen (1992)

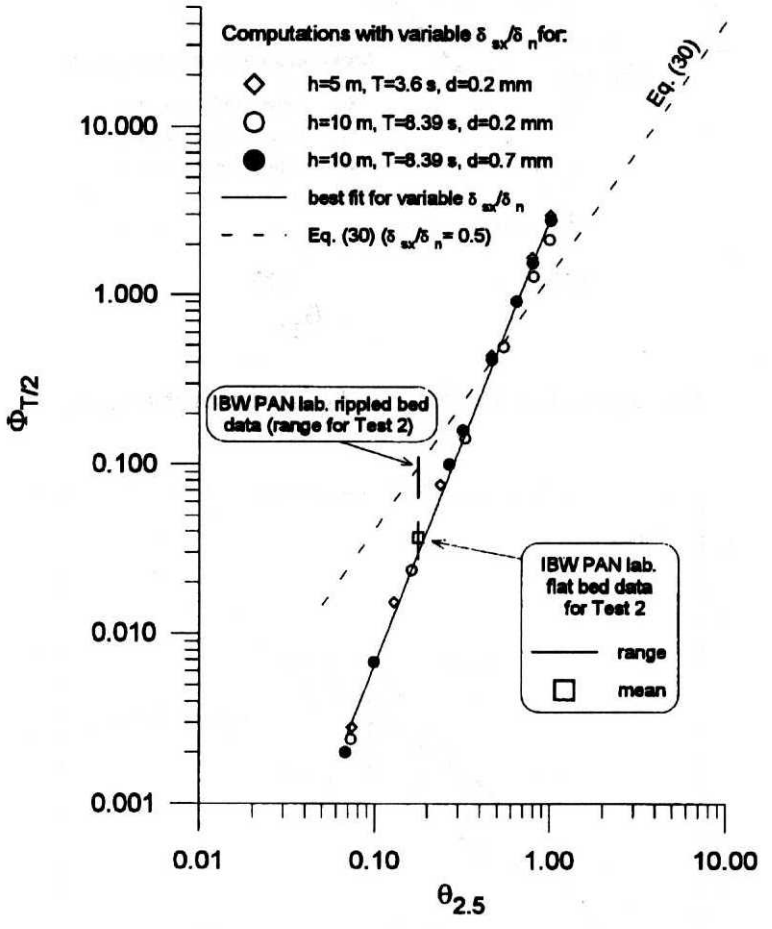

Fig. 10a. Bedload transport rate on rippled and artificial flat beds: model values vs. IBW PAN laboratory data

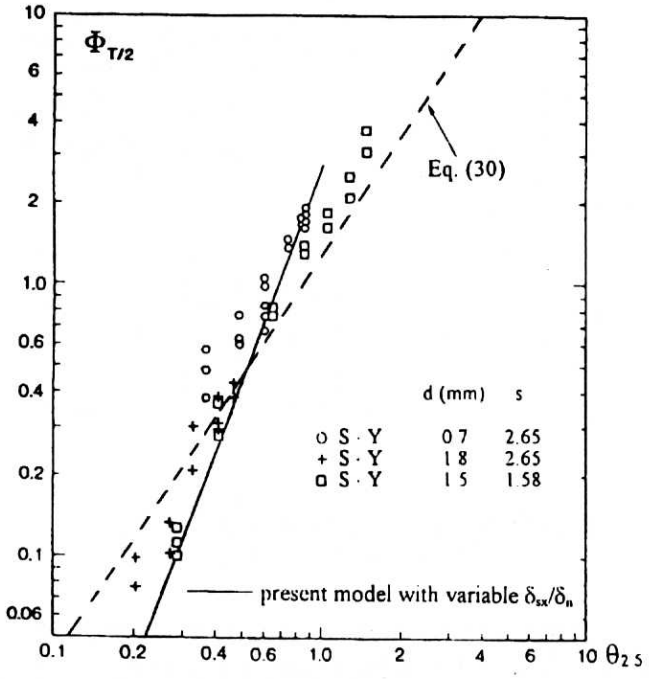

Fig. 10b. Bedload transport rate on a flat bed: model values vs. Sawamoto & Yamashita's (1986) laboratory data

in which

$$\theta_{\max}(d) = \frac{u_{f\,\max}^2(d)}{(s-1)gd} \tag{34}$$

is the Shields parameter obtained from the maximum shear stress ($\rho u_{f\,\max}^2(d)$) based on grain-size bed roughness, i.e. for $k_e = d$. Fig. 11 shows a realistic fit to the laboratory data.

7. Bedload Concentration in Sheet Flow Regime

The comparison of the model dimensionless bedload rate with laboratory data for total sediment transport rate presented in Figure 4b shows that at high flow intensities the data points lie significantly above the theoretical curve. This is due to the increasing importance of suspended transport. Figure 4b implies that the suspended load is about five times larger than the bedload evaluated by the present model. According to the discussion in the previous sections, it is, however, assumed that the present bedload model is still valid in sheet flow conditions. This is further confirmed by the results of model computations for concentration in the

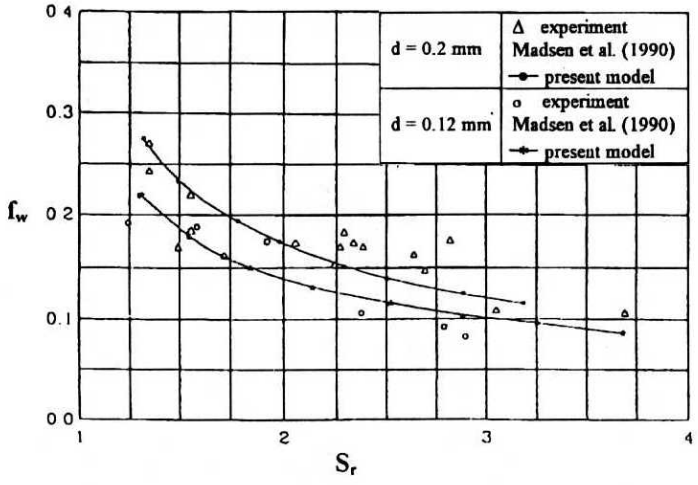

Fig. 11. Comparison of model ($\delta_{sx}/\delta_n = 0.50$) and measured wave friction factors, experimental data after Madsen et al. (1990)

collision-dominated layer for conditions appropriate to the sheet flow experiments of Ribberink & Al-Salem (1995) which were carried out in the large oscillating water tunnel of Delft Hydraulics.

Figure 12a shows the model concentration ($c, g/l$) results in the bedload layer for $\delta_{sx}/\delta_n = 0.50$ compared with measured concentrations at three levels. Ribberink & Al-Salem's (1995) condition 1 has been used. The movement of grains with $d = 0.21$ mm took place under asymmetric oscillatory motion (see velocity plot (u) at the top of Fig. 12a), with $U_{rms} = 0.6$ m/s and $T = 6.5$ s. The input free stream velocity in the theoretical model has been represented in terms of a 2nd order Stokes wave. Model results in Fig. 12a comprise only the time sectors in which – according to Equations (21) and (22) – the sediment movement occurs. In addition, the model vertical concentration and velocity distributions at the phases of wave crest and trough are compared with measured values in Figure 12b. The experimental data for the ordinates 0.5 mm and 1.5 mm below the theoretical bed level have been extrapolated from the original plot (laboratory results in Fig. 12a after Ribberink & Al-Salem).

The agreement between computed and measured data in Figures 12a and 12b is quite good, although the theoretical results show a flatter trend in the concentration time series. The anti-phase behaviour of bedload concentration with respect to sediment concentration in the upper layers and asymmetric effects are well represented by the model. However, further work is needed to include the effects of suspended load in the present model.

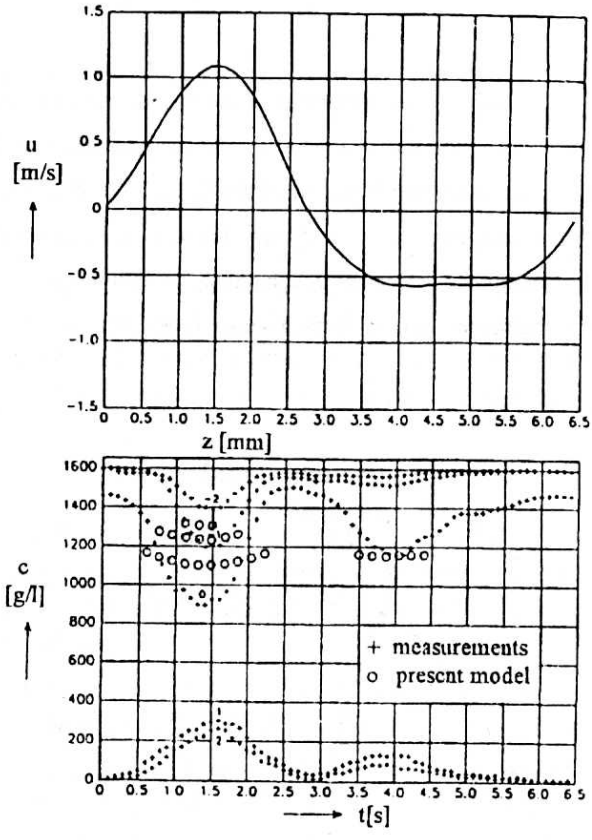

Fig. 12a. Measured and model ($\delta_{sx}/\delta_n = 0.50$) sheet flow concentrations; condition 1 of Ribberink & Al-Salem (1995)

8. Conclusions

An existing model of sheet flow sediment transport has been used to predict bed roughness and sediment transport rates for a range of low and high wave conditions. The bedload sediment transport model is based on a collision-dominant drag concept and uses a single parameter, δ_{sx}, to define the theoretical level of the top of the moving bedload layer in relation to the effective roughness height of the above-bed wave-induced flow. The value δ_{sx} is set as an arbitrary fraction of the depth of the moving bedload layer δ_n. Comparison of model results against a range of laboratory experiments shows that model as capable of producing realistic values of observed drag and sediment transport rates at low wave conditions provided a variable value of $\delta_{sx}/\delta_n \leq 0.50$ is used. At high wave conditions corresponding to sheet flow, realistic values of drag and bed sediment transport rate were obtained, as well as concentration values with wave phase using a fixed value

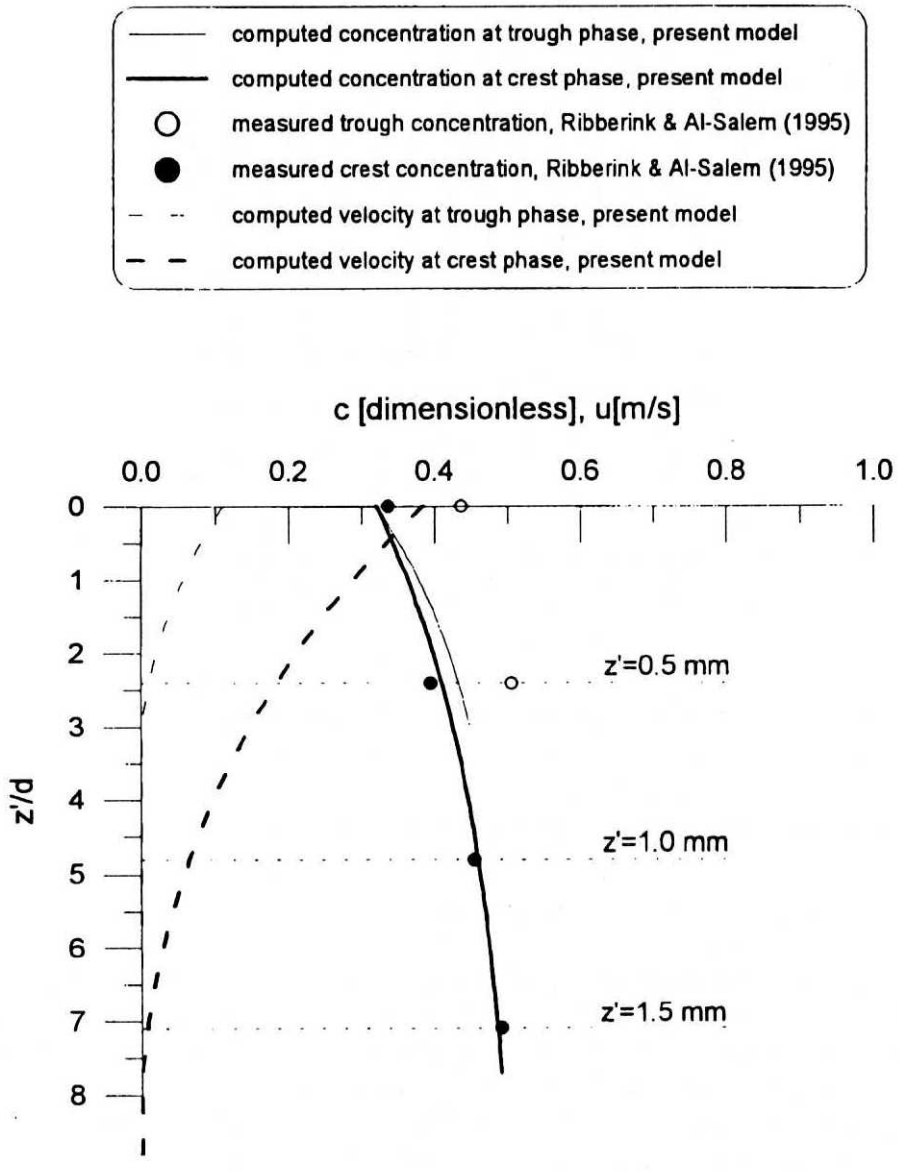

Fig. 12b. Model ($\delta_{sx}/\delta_n = 0.50$) vertical concentration and velocity distributions for phases corresponding to the time of wave crest and trough in comparison with measured values of concentration from Ribberink & Al-Salem (1995)

of $\delta_{sx}/\delta_n = 0.50$. However, model modification is needed to introduce the effect of suspended load. Finally, despite that the model does not explicitly include the drag produced by bed forms at low wave conditions, using δ_{sx}/δ_n value equal to 0.50 allows to compensate the drag and to predict realistic values of bed roughness and sediment transport.

9. Acknowledgements

The authors are grateful for the financial support provided under the Polish Scientific Research Committee and British Council programmes which enabled this work to be completed. The authors also wish to thank the Royal Society, London, for initial funding of a Postdoctoral Fellowship, which enabled L. M. Kaczmarek to work as an Honorary Research Fellow in the Department of Civil Engineering at the University of Liverpool.

References

Bagnold R.A. (1954), Experiments on a gravity-free dispersion of large solid spheres in a Newtonian fluid under shear, *Phil. Trans., R. Soc.,* London, Ser. A, 225, 49-63.

Bagnold R.A. (1956), The flow of cohesionless grains in fluids, *Phil. Trans., R. Soc.,* London, Ser. A, 249 (964), 235-297.

Brevik I. (1981), Oscillatory Rough Turbulent Boundary Layers, *J. Wtrway., Port, Coast. and Oc. Eng., ASCE,* Vol. 107, No. 3, 175-187.

Einstein H. A. (1950), The bed load function for sediment transportation in open-channel flows, *Tech. Bull.,* 1024, U.S. Soil Conserv. Serv., Washington, D.C.

Engelund F. and Fredsøe J. (1976), A sediment transport model for straight alluvial channels, *Nord. Hydrol.,* 7, 293-306.

Fredsøe J. (1984), Turbulent boundary layer in combined wave-current motion, *J. Hydraulic Eng., ASCE,* Vol. 110, No. HY8, 1103-1120.

Horikawa K., Watanabe A. and Katori S. (1982), Sediment transport under sheet flow condition, *Proc. 18th Coastal Eng. Conf., ASCE,* Cape Town, South Africa, 1335-1352.

Jonsson I. G. and Carlsen N. A. (1976), Experimental and theoretical investigations in an oscillatory turbulent boundary layer, *J. Hydraul. Res.,* Vol. 14, No. 1, 45-60.

Kaczmarek L. M. (1991), Mathematical model for oscillating sheet flow, *Proc. Euromech 262 Colloquium, Sand Transport in Rivers, Estuaries and the Sea,* Wallingford 1990, edited by Soulsby R. & R. Bettess, 197-202.

Kaczmarek L. M., Harris J. M. and O'Connor B. A. (1994), Modelling moveable bed roughness and friction for spectral waves, *Proc. 24th ICCE, 300-314, ASCE,* New York.

Kaczmarek L. M. and O'Connor B. A. (1993a, b), A new theoretical approach for predictive evaluation of wavy roughness on a moveable flat/rippled bed, Parts I/II, *Reps. CE/14-15/93, Dept. Civ. Engng., Univ. Liverpool.*

Kaczmarek L. M. and Ostrowski R. (1992), Modelling of wave-current boundary layer in the coastal zone, *Proc. 23rd Intern. Conf. Coast. Eng., ASCE,* 350-363.

Madsen O. S., Mathison P. P. and Rosengaus M. M. (1990), Moveable bed friction factors for spectral waves, *Proc. 22nd Intern. Conf. Coast. Engng.,* 420-429, ASCE, New York.

Nielsen P. (1992), Coastal bottom boundary layers and sediment transport, Advanced Series on Ocean Engineering, Vol. 4, World Scientific, Singapore.

Ribberink J. S. and Al-Salem A. (1992), Time-dependent sediment transport phenomena in oscillatory boundary layer flow under sheet flow conditions, *MAST-Conference,* Pisa, Italy.

Ribberink J. S. and Al-Salem A. (1995), Sheet flow and suspension of sand in oscillatory boundary layers, *Coastal Engineering,* No. 25, 205-225.

Sawamoto M. and Yamashita T. (1986), Sediment transport rate due to wave action, *J. Hydroscience and Hydraul. Eng.,* Vol. 4, No. 1, 1-15.

Sayed M. and Savage S. B. (1983), Rapid gravity flow of cohesionless granular materials down inclined chutes, *J. Applied Mathematics and Physics (ZAMP),* Vol. 34, 84-100.

Sumer B. M., Kozakiewicz A., Fredsoe J. and Deigaard R. (1996), Velocity and concentration profiles in sheet-flow layer of movable bed, *J. Hydraulic Eng.,* Vol. 122, No. 10.

Van Rijn L. C. (1993), Principles of sediment transport in rivers, estuaries and coastal seas, *Aqua Publications,* the Netherlands.